VOLUME 37 NUMBER 1 JANUARY 2010 ISSN 0267-8292

Liquid Crystals

an international journal of science and technology

Image provided by Rego *et al.*, taken from Asymmetric synthesis of a highly soluble 'trimeric' analogue of the chiral nematic liquid crystal twist agent Merck S1011

Editor: Corrie T. Imrie

Taylor & Francis
Taylor & Francis Group

Recognized by the European Physical Society

Liquid Crystals,
Vol. 37, No. 1, January 2010, 1–11

Taylor & Francis
Taylor & Francis Group

The kinetics of photo-polymerisation in the fabrication of polymer-dispersed liquid crystals doped with nano-graphite

J.H. Wang, B.Y. Zhang*, W.Z. Qu, H.S. Chu and H. Li

The Centre for Molecular Science and Engineering, Northeastern University, Shenyang 110004, People's Republic of China

(Received 14 February 2009; final form 27 August 2009)

It is known that the electro-optical behaviour of polymer-dispersed liquid crystals depends on the separation of the polymer and liquid crystal phases. The morphology of the liquid crystal domains depends on the nature of the chemical and physical processes occurring during domain formation. This work discusses the two-phase morphology found in an acrylate-based system that develops during polymerisation-induced phase separation. The effect of the dopant nano-graphite on the polymerisation and electro-optical properties are discussed. UV/VIS and time-resolved Fourier transform infrared spectroscopy is used for monitoring the polymerisation of the polymer-dispersed liquid crystals. The electro-optical properties of the polymer-dispersed liquid crystal films are measured using a polarimeter (PerkinElmer Model 341). The morphology of the liquid crystal droplets in the polymer matrix is probed by polarising optical microscopy and Fourier transform infrared spectroscopy images. The threshold voltage of the polymer-dispersed liquid crystals is dramatically decreased because of the increased conductivity of the polymer matrix on doping by nano-graphite.

Keywords: kinetic photo-polymerisation; real-time transmittance; electrooptical; FTIR images; morphology

1. Introduction

Polymer-dispersed liquid crystals (PDLCs) are polymer/liquid crystal (LC) composite materials proposed for applications in switchable windows and imaging technology due to their unique electro-optical performance characteristics [1–25]. Since the original reports of these materials, researchers have extensively examined PDLC formation, seeking optimised performance. Much of this work has focused on correlating PDLC morphology to performance parameters such as on-state transmittance, off-state scattering and switching voltage.

PDLCs are often formed through polymerisation-induced phase separation (PIPS), a one-step fabrication technique, in which a polymerisation initially occurs in an isotropic mixture of LCs and monomers. The formation of PDLCs is typically induced by photo-polymerisation (UV-curing) [3]. On polymerisation, the LCs lose solubility in the polymer and separate into a distinct phase through either liquid–liquid or liquid–gel demixing. Upon phase separation, PDLCs take one of two morphologies: droplets ('Swiss cheese') or interconnected (polymer ball) [26]. PDLCs form droplets or an interconnected morphology based on LC concentration, polymerisation mechanism, polymerisation kinetics and polymer composition [26].

The electro-optical performance characteristic is an important factor in optimising the performance of PDLCs. To optimise the electro-optical performance of PDLCs, nano-composites, surfactants and dyes have been used as dopants in PDLCs [27]. The dielectric constant and morphology of PDLCs are important parameters to optimise the electro-optical performance. On increasing the dielectric constant, the threshold voltage is decreased and the energy consumption is reduced. In typical PDLC systems, the sizes of the LC domains are of the order of micrometres. These cause an intense scattering of light in the visible range and the values of the switching voltage are of a few tenths of volts [28]. By increasing the efficiency of the phase separation process, which depends on the component concentration and UV-curing parameters, submicrometre (nano-sized) droplets can be obtained. As a consequence, the PDLC samples are characterised by low light scattering and high optical transmission. However, by applying a suitable voltage, it is possible to affect the orientation of the LCs, thus changing the average refractive index of the medium. It has been demonstrated that phase-only modulation is possible without any important dependence on the light polarisation [28]. This occurs when light impinges at normal incidence, since in this case the light wave vector has the direction of the external applied field, i.e. of the optic axis of the medium. Under this propagation condition, the light travels into the medium as an ordinary wave regardless of its polarisation state. For this reason, nano-size PDLCs are potentially of strong interest for the development of innovative devices for optical communication technology.

In this article, we report a detailed investigation performed on micro-size PDLCs obtained by using a

*Corresponding author. Email: baoyanzhang@hotmail.com

ISSN 0267-8292 print/ISSN 1366-5855 online

multifunctional monomer in a pre-polymer mixture that is suitable for a fast polymerisation process. In particular, we have investigated nano-graphite doped materials, paying particular attention to the polymerisation kinetics in phase separation and electro-optical properties. In the following, the electro-optical property of PDLCs film is studied. Finally, we describe the morphology of LCs in the polymer matrix, which have been characterised by polarising optical microscopy (POM) and three dimensional Fourier Transform Infrared (3D-FTIR) images in detail.

2. Experiments

2.1 Materials

Epoxy acrylate (EA), initiator (1173) and cross-linking trimethylolpane triacrylate (TMPTA) were purchased from Tianjin Tianjiao Chemical Company of China. The LC 76G9700 was supplied by Shijiazhuang SLICHEM material company. TMPTA is a transparent liquid whose refractive index is 1.4723. Nematic LC 76G9700 is a eutectic mixture of cyanobiphenyl and cyanoterphenyl ($n_0 = 1.49$, $\Delta n = 0.15$, $T_{N-I} = 122°C$). Nano-graphite was purchased from Qingdao Huatai Lubricant Sealling S&T. Co. Ltd. of China and the size is 500 nm.

2.2 The PDLC formulations

All formulations examined contain 1% initiator 1173, different mass ratios of nano-graphite and 76G9700. Most PDLC formulations in this report contain the EA, trifunctional monomer TMPTA and nano-graphite. The effect of nano-graphite on the electro-optical property of the LC droplets is investigated. The compositions of the PDLC formulations studied here are listed in Table 1.

Table 1. Summary of PDLC mixtures with different component ratios.

Mixture	TMPTA[a]	EA[a]	Nano-graphite %[b]	Sample	LC[c]	Initiator %[d]
A	2	1	0	A1	40	1
				A2	30	1
B	2	1	0.05	B1	40	1
				B2	30	1
C	2	1	0.1	C1	40	1
				C2	30	1
D	2	1	0.2	D1	40	1
				D2	30	1

[a]The ratio of TMPTA/EA. [b]The ratio of nano-graphite/(TMPTA + EA + nano-graphite)×100%. [c]The ratio of LC/mixture. [d]The ratio of initiator/(LC + mixture + initiator) ×100%.

2.3 Methods

FTIR spectroscopy is an easily accessible, direct and non-invasive method of examining chemical changes and has been applied to study PDLC formation [29–33]. The FTIR method has been used as an important method for characterising the photo-polymerisation kinetics of UV-curable coatings from the very inception of the discovery and development of photo-induced polymerisations. The effect of the LC content and of the nano-graphite dopant on the kinetics of polymerisation was monitored by real-time FTIR spectroscopy (PerkinElmer spectrum one). The double bond conversions of the pre-polymer were monitored in real-time FTIR under UV-curing. A UV/VIS spectrometer was adapted to enable a real-time study of the speed of the photo-polymerisation and how it is affected by LC content and by the nano-graphite dopant. Samples were sandwiched between two indium tin oxide (ITO) glass substrates separated by 10 μm spacers. Photo-polymerisation was initiated by a UV light (10 W). Spectra were collected every 0.2s during the polymerisation process. The change of transmittance versus time was collected with different samples.

Electro-optical properties of fabricated PDLC films were measured using a polarimeter (PerkinElmer Model 341). PDLCs were polymerised between two ITO glass slides with a spacer of 10 μm. The transmittance of light through the PDLCs was set at 589 nm and the voltage (sine wave, 50 Hz) was increased stepwise until the PDLCs became most transparent.

POM and FTIR with mercury cadmium telluride (MCT) detector were used to directly examine the polymer/liquid crystal morphology. PDLC formulations were polymerised between glass microscope slides with 10 μm spacers. The FTIR images were collected to study the morphology of polymer/LCs when the films were flayed from the glass microscope slides. FTIR images were collected at 6.25 μm resolution during the process of scanning. The MCT was cooled by liquid nitrogen.

3. Results and discussion

3.1 Effect of the concentration of liquid crystals and the nano-graphite dopant on kinetics

The trajectory of the samples through phase space as it undergoes phase separation in PIPS is complex, as the system may be thrust from metastable to unstable regions as the polymerisation proceeds [34]. As the system enters the metastable region, newer domains may form between the existing domains due to heterogeneous nucleation, thus the

inter-domain distance could become smaller with the progress of the polymerisation process. There may be a cross-over from nucleation to spinodal decomposition, as the coexistence line passes through the metastable region before reaching the unstable region as the polymerisation proceeds [35]. A further complexity arises from the fact that supercooling (the difference of temperature between the coexistence line and the reaction temperature) increases as the polymerisation proceeds, which in turn can make the domains smaller. This process may compete with the intermediate stage of spinodal decomposition which grows the domain size to create a Cahn-Hilliard linear region that is longer than expected [36].

Time-resolved light scattering experiments were performed at 130°C using an instrument based on the UV/VIS spectrometer (PerkinElmer Lambda 950). The probe beam, fixed at 623.18 nm, passes through a pinhole held perpendicular to the sample. Scattering data for all the experiments are collected continuously every 0.2 s over 2000 s periods throughout the process of each experiment. The data were plotted as transmittance versus the curing time. The curing beam is produced by an UV light (10 W). In order to ensure the uniform illumination of the sample, we employ the UV light at a distance of 10 cm with an incidence angle of 60°. Representative light scattering profiles for the process of phase separation for both 40% and 30% content of LCs samples with different levels of nano-graphite dopant are given in Figures 1(a)–1(d). From the scattering data in Figure 1, we observe features that are shared by both LC compositions studied and reveal more details regarding

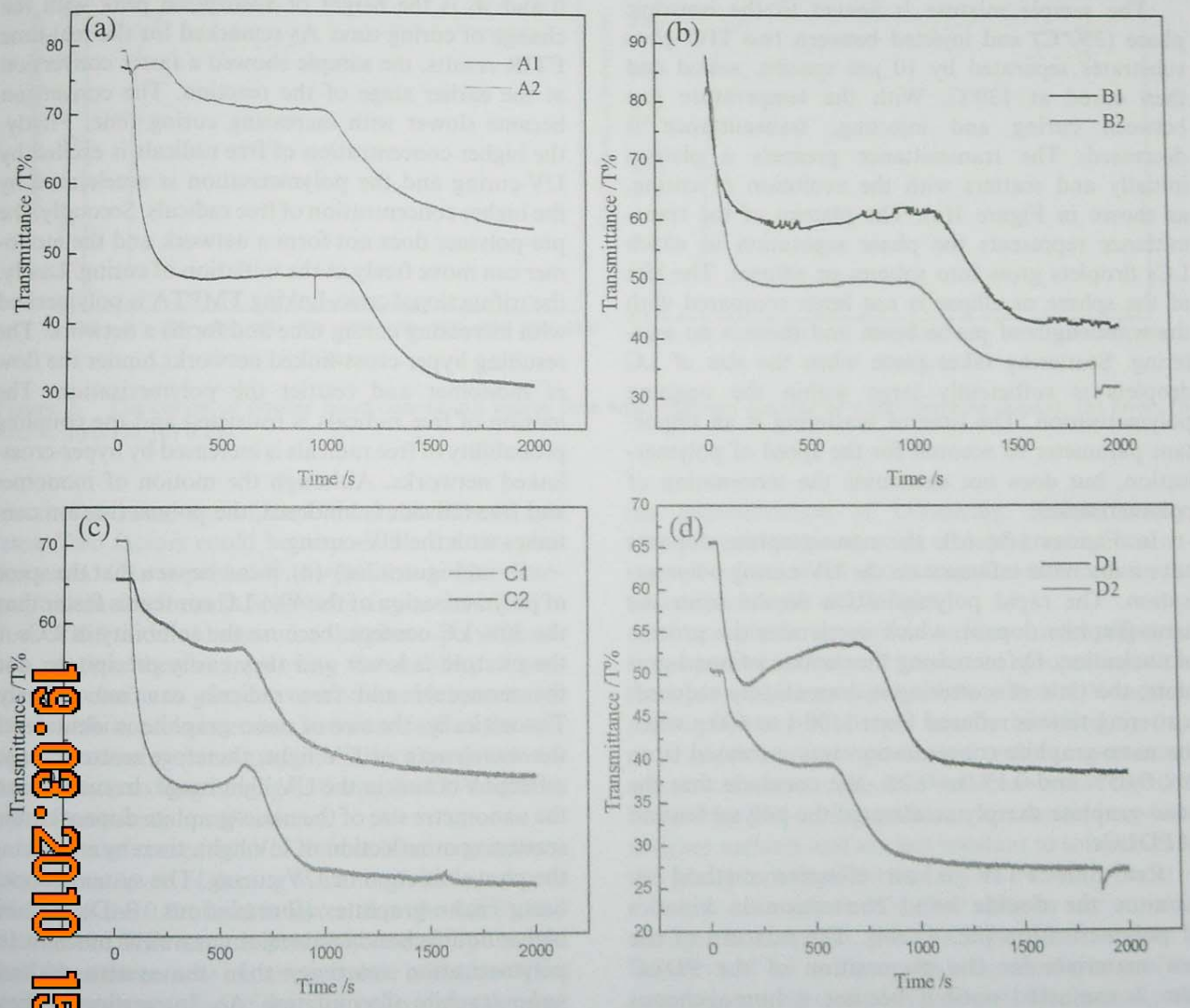

Figure 1. The curves of transmittance versus time with different content of nano-graphite dopant, (a) none, (b) 0.05%, (c) 0.1% and (d) 0.2%.

the phase separation mechanism. One feature common to both compositions is the delay time between the start of the experiment and the appearance of a maximum scattering. This gap, called the induction period [37–41], corresponds to the delay in phase separation from the growth of the polymer matrix. In other words, for the system to favour phase separation of the blends into LC-rich and gel-rich domains, the polymerisation must generate matrix material of sufficiently large molecular weight to induce thermodynamic instability. The second feature common to both blends has to do with the appearance of a single maximum in the scattering that not only grows in intensity but also changes in scattering with time. Lastly, when the scattering profiles no longer change, the phase separation process has not been effectively arrested, an event where the LC droplets grow large enough to exceed the probe wavelength and do not scatter.

The sample mixture is heated to the isotropic phase (150°C) and injected between two ITO glass substrates separated by 10 μm spacers, sealed and then cured at 130°C. With the temperature gap between curing and injecting, transmittance is decreased. The transmittance presents a plateau initially and scatters with the evolution of curing, as shown in Figure 1(a). The plateau of the transmittance represents the phase separation in which LCs droplets grow into spheres or ellipses. The size of the sphere or ellipse is not large compared with the wavelength of probe beam and there is no scattering. Scattering takes place when the size of LC droplets is sufficiently large within the ongoing polymerisation. The time of scattering is an important parameter to account for the speed of polymerisation, but does not determine the termination of polymerisation.

In Figures 1(b)–(d), the nano-graphite dopants have a dramatic influence on the UV-curing polymerisation. The rapid polymerisation results from the nano-graphite dopant, which accelerates the process of nucleation. On increasing the content of nano-graphite, the time of scattering is dramatically reduced; scattering time is reduced from 1100 s to 600 s when the nano-graphite concentration was increased from 0%, 0.05% to 0.1% to 0.2%. We conclude that the nano-graphite sharply accelerated the polymerisation of PDLCs.

Real-time FTIR is an effective method to monitor the double bond conversion in kinetics of polymerisation [32, 42–44]. The mixture of the raw materials for the preparation of the PDLC film is sonicated until it became a homogeneous syrup. The mixture is sputtered onto a piece of potassium bromide disc and covered with further potassium bromide at 150°C. The spacer is determined by the polymer film, which is 10 μm. To avoid the influence of oxygen, the boundary of sample cell is packed by a polytetrafluoroethylene film and UV-curing is under a nitrogen atmosphere. The sample cell is equipped at the beam of FTIR for collecting the spectrum with the process of polymerisation.

The double bond conversion is plotted as a function of curing time in Figures 2(a)–(d). The double bond conversion at 1635 cm^{-1} is monitored with the evolving polymerisation. The double bond conversion $\eta_{C=C}$ is calculated as shown [45]:

$$\eta_{C=C} = \frac{A_0 - A_t}{A_0} \tag{1}$$

where A_0 is the height of initial absorption peak at $t = 0$ and A_t is the height of absorption peak with the change of curing time. As remarked for the real-time FTIR results, the sample showed a faster conversion at the earlier stage of the reaction. The conversion became slower with increasing curing time. Firstly, the higher concentration of free radicals is excited by UV-curing and the polymerisation is accelerated by the higher concentration of free radicals. Secondly, the pre-polymer does not form a network and the monomer can move freely at the initiation of curing. Lastly, the trifunctional cross-linking TMPTA is polymerised with increasing curing time and forms a network. The resulting hyper-cross-linked networks hinder the flow of monomer and restrict the polymerisation. The motion of free radicals is restricted and the coupling probability of free radicals is increased by hyper-cross-linked networks. Although the motion of monomer and free radicals is hindered, the polymerisation continues with the UV-curing.

From Figures 2(a)–(d), it can be seen that the speed of polymerisation of the 40% LC content is faster than the 30% LC content, because the solubility of LCs in the mixture is lower and they easily precipitate, and the monomer and free radicals can move freely. Theoretically, the size of nano-graphite is identical to the wavelength of UV light, therefore scattering and reflection occurs in the UV light range. In such a case, the nanometre size of the nano-graphite dopant causes scattering or reflection of UV light, thereby enhancing the photoinitiation of UV-curing. The systems doped using nano-graphite (formulations B–D) exhibit higher double bond conversions as well as much faster polymerisation reactivity than the system without nano-graphite (formulation A). Interestingly, these results indicate that the presence of nano-graphite apparently accelerated rather than hindered the cure

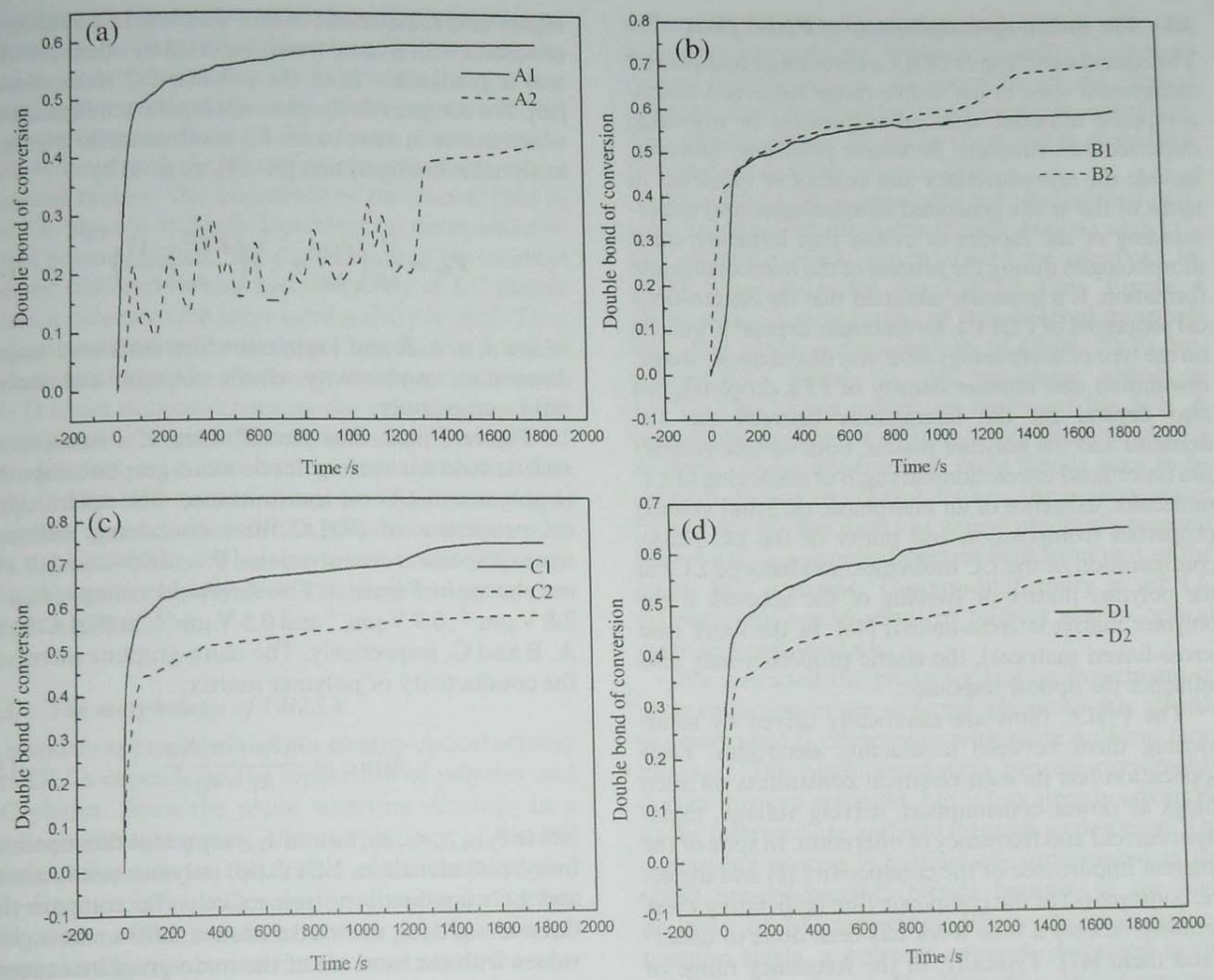

Figure 2. The curves of double bond conversion versus time with different content of nano-graphite dopant, (a) none, (b) 0.05%, (c) 0.1%, (d) 0.2%.

reaction and cure rate of the UV-curable PDLCs systems. Two factors could be responsible for this phenomenon. One is probably attributable to the nano-graphite in the formulations behaving as an effective flow or diffusion-aid agent for the photo-polymerisation process, thereby improving the mobility of propagating chains to give rise to a noticeable increase in the double bond conversion and cure rate of the systems doped using nano-graphite. The other could be a contribution to lengthening of the path of UV light by partial scattering or reflection.

From the comparison of double bond conversions for different levels of doping by nano-graphite, we conclude that the 0.2% level is lower than the 0.05% and 0.1% levels. This result is probably caused by the fact that, when the content of nano-graphite is increased, the aggregates grow to larger than nanometre size, hindering the absorption of the incident radiation by the photoinitiator and thereby reducing the efficiency of the photoinitiation of UV-curing. Simultaneously, with increased concentration of nano-graphite, scattering and reflection are also increased, which reduces the transmitted depth of UV light.

Atmospheric conditions have a drastic effect on the physicochemical and mechanical properties of the final product. In particular, free-radical UV-induced photo-polymerisations are usually inhibited by oxygen and often must be performed under an inert atmosphere such as nitrogen. It is well known that the films formed by UV-curing under an air atmosphere have rougher surfaces and are less resistant to solvents than the glassy coatings formed by UV-curing under a nitrogen atmosphere [33]. Our samples are cured in nitrogen atmosphere, except sample A2. As shown in the curve of A2 in Figure 2(a), the atmosphere of the sample is not injected with nitrogen. The rate of polymerisation is fluctuant increased for the influence of oxygen.

3.2 The electro-optical property of PDLC films

The optical switching of PDLCs between an opaque and transparent state in the visible range requires a microcomposite material with submicrometre or microsize dispersed LCs droplets. Persistent problems, however, include the reproducibility and control of materials in terms of the *in situ* generated morphologies and understanding of the factors or events that influence these morphologies during the process of the microcomposite formation. It is generally admitted that the electro-optical properties of PDLCs, for example, depend primarily on the type of morphology (size, size distribution, shape, orientation and number density of LCs droplets), but also depend on the interactions between the LC domains and the polymer matrix, both surface properties (interfacial interactions/strength of anchoring of LC molecules, existence of an interphase, etc.) and volume properties (composition and purity of the LC phase, configuration of the LC molecules, solubility of LCs in the polymer matrix or swelling of the network if the polymer matrix is cross-linked) [46]. In the latter case (cross-linked matrices), the elastic properties may also influence the optical response.

The PDLC films are electrically driven by sandwiching them between conducting electrodes. Each application has its own electrical constraints on such things as power consumption, driving voltage, maximum current and frequency of operation. In spite of the inherent importance of the conductivity (δ) and dielectric constant (ε) of the composite film in dictating these parameters, only a little work has been done to understand them [47]. Typically, in the frequency range of interest for polymer/LC-composed films' operation, the strength of an AC electric field is modulated by the frequency of the imposed AC electric field. Since electronic and ionic polarisation mechanisms are very far from their resonances, which occur at or above infrared frequency region, only permanent dipole resonances resulting from molecular reorientation are related to PDLC film operation. These resonances of the interfacial polarisation occur in conjunction with changes in the dielectric constant and conductivity [47]. It has been reported that the polymer matrix with greater magnitude of conductivity leads to enhancement of the electro-optical response speed [48, 49]. Here, we prepared a new polymer/LCs composite film employing nano-graphite as a dopant in polymer matrix TMPTA/EA substitutes. Polymer matrix exhibits high conductivity when it contains the nano-graphite. It has a high optical transparency and high conductivity. In this paper, we discuss the influence of the conductivity of the polymer matrix on the electro-optical properties of the PDLC.

The threshold voltage (V_{th}) is defined as voltage when the transmittance reach at 10% of maximum. The higher field requirement of film with low LCs loading is consistent with general trends reported by others [49–50] and is predictable from the polymer-LC series model [50]. For comparable droplets size bipolar configuration, which occurs in most cases, V_{th} is substantially less than in alphabet configuration [51–53], as given by

$$V_{th} = \frac{d}{3a}\left(\frac{\delta_{LC}}{\delta_P} + 2\right)\left(\frac{K(l^2-1)}{\varepsilon_0 \Delta\varepsilon}\right)^{1/2} \tag{2}$$

where d, a, δ, K and l represent film thickness, major dimension, conductivity, elastic constant and aspect ratio, respectively.

Figure 3 illustrates the influence of a function of electric field for various levels nano-graphite dopants in polymer matrix on transmittance. The electro-optical properties of PDLC films containing different nano-graphite concentrations 0%, 0.05% and 0.1% are shown in Figure 3. The threshold voltage (V_{th}) is 2.8 V μm^{-1}, 0.9 V μm^{-1} and 0.5 V μm^{-1}, in PDLC films A, B and C, respectively. The nano-graphite increases the conductivity of polymer matrix:

$$\delta_{PDLC} = \frac{n_1\delta_P + n_2\delta_{LC}}{n_1 + n_2} \tag{3}$$

where δ_{PDLC}, n_1, n_2, δ_P and δ_{LC} represent film conductivity, polymer ratio, LCs ratio, polymer conductivity and LCs conductivity, respectively. To compare the three sets of data, the transmittance shifts to the higher values with the increase of the nano-graphite concentration because the ordinary refractive index of the LC

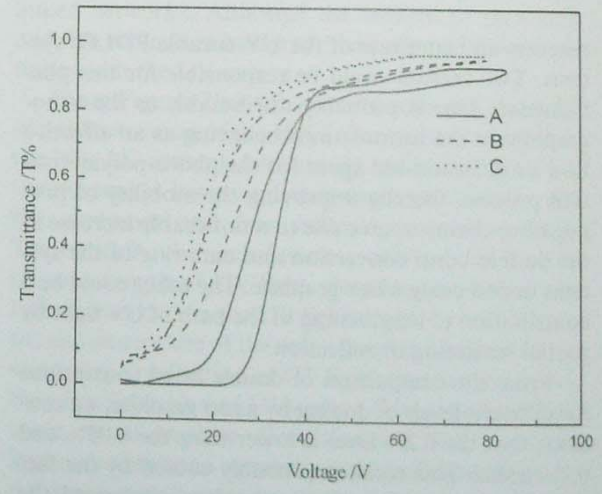

Figure 3. The curves of transmittance as a function of electric field for various nano-graphite dopant ratios (A, 0%; B, 0.05%; C, 0.1%) at 20°C and 50 Hz.

matches more closely with that of the polymer. Threshold voltage (V_{th}) decreases with increasing nano-graphite ratio. This result is related to the fact that the increased conductivity of the polymer matrix leads to decrease of threshold voltage. V_{th} is remarkably reduced with the increasing of conductivity of the polymer matrix. The magnitude of the electric field in the LC phase is strongly dependent on the conductivity of polymer matrix. The distribution of the external electric field can be imposed effectively to LC phases when a polymer with large conductivity is used. Thus the polymer matrix with larger conductivity led to reduction of V_{th}. The electro-optical property of sample D is not discussed because the aggregation of the nano-graphite dopant disarranged the dispersion of LC droplets in a non-homogeneous manner. The PDLC film D is broken down for the higher nano-graphite concentration in the polymer matrix under the applied voltage. The upper and lower ITO substrates were electrically short-circuited by aggregation of nano-graphite.

3.3. *The morphology of PDLCs*

It is widely appreciated that the electro-optical activity in PDLCs depends on the separation of polymer and LC phases. Since the phase structure develops in a non-equilibrium system, the morphology of the LC domains depends on the details of the chemical and physical processes active during domain formation. The nature of the interface between polymer and LC phases is of particular interest. In most cases, the two-phase morphology that results falls into one of two categories: a 'Swiss cheese' morphology, where spherical LC droplets are embedded in polymer matrix, or a 'reverse morphology', where a continuous LC phase is embedded in polymer bead-like matrix [27, 53]. In the latter case, the LC phase does not have droplet character. Controlling LC domain morphology is important since it modulates the electro-optical properties of PDLCs [54–55].

The performance of PDLCs strongly depends on the final morphologies, sizes, distribution and shapes of phase-separated LC domains. The size can be controlled by adjusting the kinetics of polymerisation and the phase separation of LCs during the polymerisation, which depends on experimental conditions (such as exposure beam intensity and exposure time), concentration and physical properties (such as viscosity of LCs and the chemical structures of reactive diluents) [56]. Three factors are estimated to determine the polymerisation-induced phase separation of an LCs from the system [57]. The first factor is the increase in the fraction of large molecules during polymerisation (size-induced phase separation). Second is the difference in the interaction parameters between monomer and polymer. When cross-linking is formed during polymerisation, the elasticity of the formed network is the third driving force for phase separation. This effect becomes strong by the increase of gel fraction and the number of cross-links.

The clearly phase-separated morphologies of periodic polymer-rich domains (bright region) and LC-rich domains (dark region) could be observed by POM observation for the PDLCs film. Figure 4 shows optical micrographs of the observed morphology after photo-polymerisation of 60/40, 70/30 pre-polymer/LCs blends in the two-phase region at 130°C. The LCs is etched by methanol for 24 h. A heterogeneous texture with unevenly distributed LCs droplets can be discerned. If these blends were to be used for display or control devices, the orientation of LCs in the smaller domains would obviously respond differently to an applied electric field from that of the larger LCs domains. The non-uniformity in the LC droplet sizes would result in inferior electro-optical switching performance.

We restricted the phase separation experiment to photoinitiation in the isotropic phase, as this affords pre-polymer/LC composites with more uniform morphology. The phase separation process presumably occurs through spinodal, but it has already advanced to the intermediate and late through coalescence. The coarsening process is particularly pronounced in the 60/40 pre-polymer/LC blends because of the high mobility of LC molecules. When the cross-linking reaction starts, a polymer network is formed in the polymer-rich regions. The formation of polymer networks presumably impedes the growth of these droplets, thereby virtually ceasing the growth. As a consequence, these droplets impinge on each other, resulting on a change of the domain topology form a spherical shape. The smaller droplets are obtained in the 70/30 pre-polymer/LC blends because of the high mobility of the pre-polymer molecules. The polymer network is rapidly formed for starts of the trifunctional cross-linking reaction. The LCs do not coalesce and grow into larger droplets, as shown in Figures 4(a2), (b2) and (c2).

With the nano-graphite dopant, the polymerisation is accelerated because of the reflection and scattering by the nano-graphite in curing light. The speed of phase separation is accelerated by the rapid polymerisation of pre-polymer and the LC droplets are not grown into larger than nano-graphite undoped mixture as shown in Figures 4(b1)–(c2). The dispersion of the LC droplets is damaged by the aggregation of the nano-graphite in the polymer matrix, as shown by the big black domain in Figures 4(d1) and (d2). The electro-optical property of the PDLC films is influenced

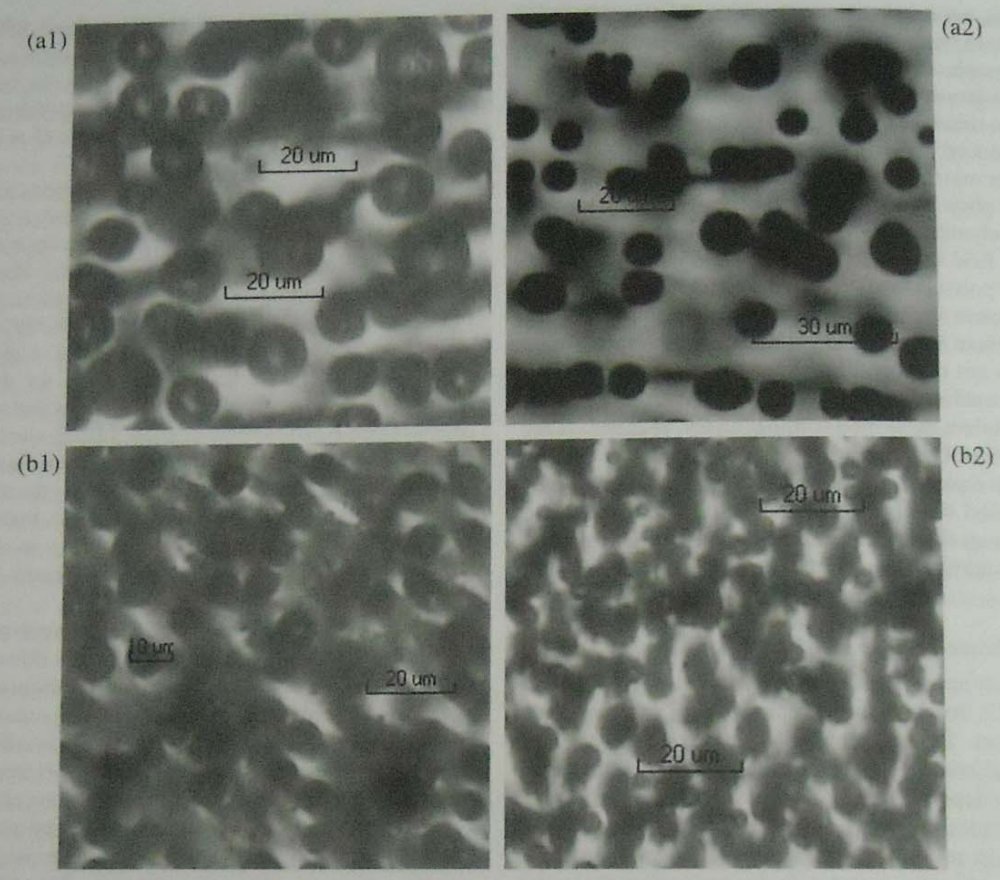

Figure 4. Optical micrographs under non-polarising light for 60/40, 70/30 prepolymer/LCs mixture showing the dependence of domain size on liquid crystal (LC) concentration after photopolymerisation ×500 (a1) 60/40, prepolymer/LC, 0% nano-graphite dopant; (a2) 70/30 prepolymer/LC, 0% nano-graphite dopant; (b1) 60/40, prepolymer/LC, 0.05% nano-graphite dopant; (b2) 70/30 prepolymer/LC, 0.05% nano-graphite dopant; (c1) 60/40, prepolymer/LC, 0.1% nano-graphite dopant; (c2) 70/30 prepolymer/LC, 0.1% nano-graphite dopant; (d1) 60/40, prepolymer/LC, 0.2% nano-graphite dopant; (d2) 70/30 prepolymer/LC, 0.2% nano-graphite dopant.

because the aggregation of the nano-graphite is embedded in LC droplets, as discussed above.

FTIR spectroscopy presents the most direct route to characterise spatial chemical variations in a sample and has been applied to PDLCs [58, 59]. By monitoring characteristic bands of a chemical species, its spatial distribution can be seen by means of a chemical image. Conventional infrared spectroscopy uses apertures to select the examined area and sequentially maps out the total spatial area. FTIR imaging using a focal plane array detector has been recently introduced [60] and successfully used for obtaining chemical images of PDLCs [61]. We used a focal plane array-equipped spectrometer to study spatial distribution of liquid crystal in PDLCs. FTIR imaging, having *in situ*, non-invasive and non-destructive examination capabilities, appears to be an excellent method to examine solubility, being constrained only by the incident radiation wavelength limited resolution.

Phase separation has been reported to occur for short polymerisation times [62–63] even when the curing is not complete. However, stable demixing is reportedly obtained at over 55% cure for the pre-polymer/LC system as discussed above. The conversion of the double bond in these experiments was of the order of over 55%. Much longer curing times would be needed to achieve a greater conversion. Since it was the intention of the study to analyse the effect of polymerisation time for a smaller curing time, this curing time and cure state achieved are considered satisfactory.

FTIR with MCT was used for directly examining the morphology of polymer/LCs. PDLCs formulations

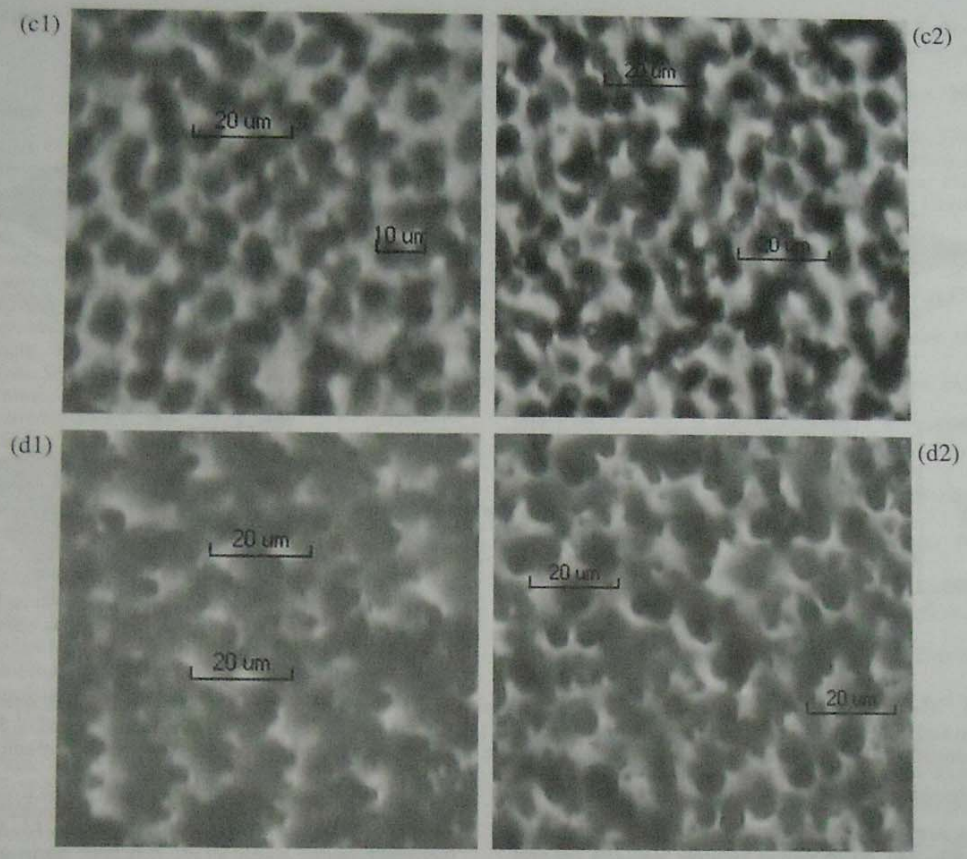

Figure 4. (*Continued*)

with 10 μm were polymerised between glass microscope slides. Afterwards the films were flayed from glass microscope slides and the FTIR images were collected to study the morphology of polymer/LCs. Spectra were collected at 6.25 μm resolution during the process of scanning. The MCT is cooled by liquid nitrogen.

Infrared images of representative samples, obtained at different contents of the nano-graphite dopant for different ratio of pre-polymer/LCs to polymerise, are shown in Figure 5. Careful attention must be paid to the manner in which IR images are plotted. In this paper, FTIR images are plotted as an area of nitrile group peak in the LCs. Area values are baseline and offset-corrected. The area is then thresholded to give the maximum absorption between regions of the sample rich and poor in the species of interest. The area representation used here not only normalises the absorption of band relative to the other but also increases the thresholding limits, making differences more prominent. All experimental data and subsequent analyses are based on sample areas away from any spacer presence. This is done to exclude thickness effects on phase separation. It is conceivable that this would lead to an equal thickness for various parts of a sample. The band absorption introduced above is based on a band specific to each component that would label intensity of component. Here, the nitrile band (2238 cm^{-1}) is used as a basis for computation and sketch of the polymer network. The intensity and dispersion of nitrile group is depicted in Figure 5.

On the scanning area, the intensity and dispersion of the nitrile group is depicted by the height of peaks. The FTIR images were obtained to illustrate the dispersion of LC domains. The size and dispersion of LC droplets are illustrated by intensity and dispersion of nitrile absorption peaks. We discuss the effect of the nano-graphite on morphology of blends 60/40, 70/30 polymer/LC in Figure 5. As the content of the LC ratio is decreased from 40 to 30, the heights and dispersion of peaks become uniform, as shown in Figures 5(a) and (b). The nano-graphite accelerates the speed of polymerisation and makes uniform the size and

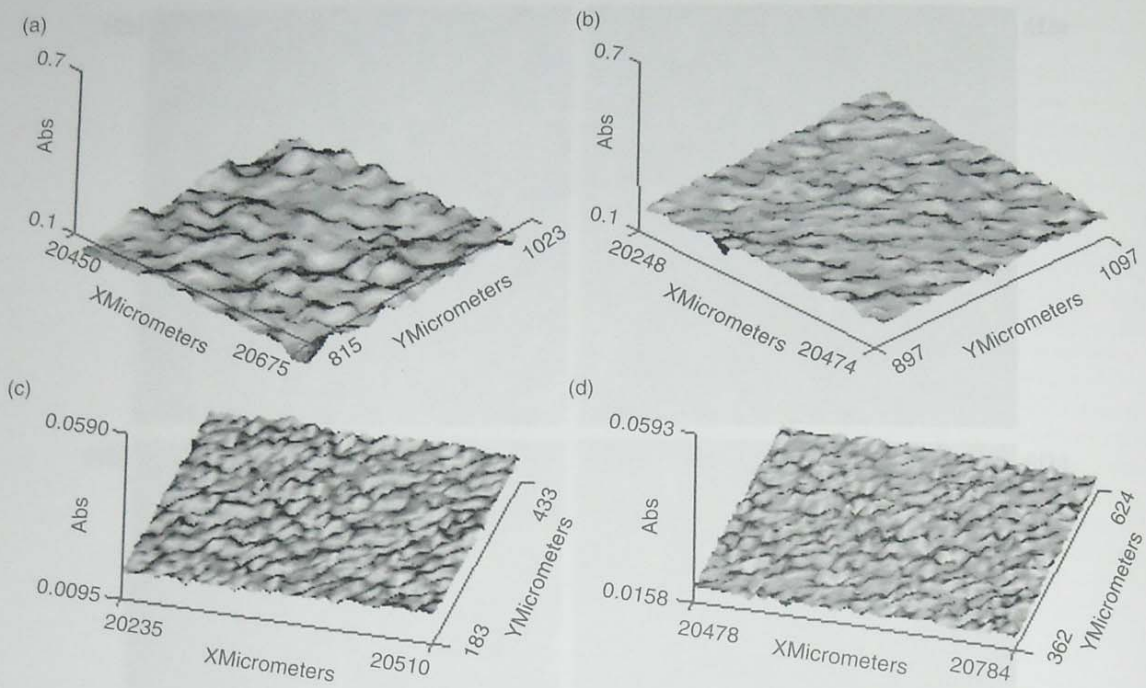

Figure 5. Fourier transform infrared spectroscopy images of polymer-dispersed liquid crystals as the area of nitrile group dispersion and intensity (a) 60/40, prepolymer/liquid crystal (LC), 0% nano-graphite dopant; (b) 70/30 prepolymer/LC, 0% nano-graphite dopant; (c) 70/30 prepolymer/LC, 0.05% nano-graphite dopant; (d) 70/30 prepolymer/LC, 0.1% nano-graphite dopant.

dispersion of LC droplets. The heights and dispersions of peaks are uniformed and smoothed as shown in Figures 5(b)–(d). As shown in Figures 5(a), (b), (c) and (d), the intensity of peaks is decreased from 0.700 to 0.547. The area of peaks is also minimised. The dispersion of peaks is uniformed due to the effect of nano-graphite. The 0.2% nano-graphite in PDLC film sample is not discussed due to its poor electric-optical property. The above analysis shows that the size and dispersion of LCs are decreased and uniformed due to effect of the nano-graphite. The same effect of the nano-graphite dopant on the morphology of blend 60/40 polymer/LC is not discussed. The solubility of LCs in the polymer matrix can be detected from the FTIR image and the phase separation does not occur significantly.

4. Conversion

The apparent reaction kinetics in double band conversion of photocurable monomers were measured via FTIR spectra. Good agreement was found between the apparent reactions kinetics from UV/VIS spectrometer and FTIR measurements. Further experiments in samples of different ratios of pre-polymer/LCs revealed that apparent kinetics in double band conversion is not only time dependent but also concentration dependent. The kinetics of double band conversion were accelerated by the nano-graphite in the mixture. The sizes and dispersion of LC droplets were influenced by different ratios of nano-graphite. The threshold electrical field was measured for different nano-graphite concentrations. The PDLC film was broken down at the ratio 0.2% of nano-graphite for the aggregation, but the ratios of 0.05% and 0.1% dramatically reduced the threshold electric field at 0.9 V μm^{-1} and 0.5 V μm^{-1}, respectively. The optimised PDLC film was obtained at 0.1% nano-graphite in the polymer matrix. The morphology of PDLC film was studied by POM and FTIR imaging. The effect of the nano-graphite on the sizes and dispersion of LC droplets in polymer matrix was depicted. The uniform sizes and dispersion of LC droplets were obtained using appropriate nano-graphite dopant levels, but the upper and lower ITO substrates were electrically short-circuited by 0.2% nano-graphite. The PDLC films were fabricated by polymerisation-induced phase separation via nucleation and growth or spinodal decomposition.

Acknowledgments

The authors are grateful to National Science Fundamental Committee of China, HI-Tech Research and development program (863), the commission for science, technology

and industry for national defence (DBDX2008038) of China.

References

[1] Odian, G. *Principles of Polymerization*, 2nd ed.; Wiley-Interscience: New York, 1981.
[2] Andrzejewska. *E. Prog. Polym. Sci.* **2001**, *26*, 605–665.
[3] Fouassier, J.P. *Photoinitiators, Photopolymerization, and Photocuring-Fundamentals and Applications*; Hauser: Munich, 1995.
[4] Kloosterboer. J.G. *Adv. Polym. Sci.* **1988**, *84*, 1–61.
[5] Sastre, R.; Conde, M.; Mateo, J.L. *J. Photochem. Photobiol. A: Chem.* **1988**, *44*, 111–122.
[6] Anseth, K.S.; Newman, S.N.; Bowman C.N. *Adv. Polym. Sci.* **1995**, *122*, 177–217.
[7] Hiratani, H.; Mizutani, Y.; Alvarez-Lorenzo, C. *Macromol. Biosci.* **2005**, *5*, 728–733.
[8] Roffery, C.G. *Photopolymerization of Surface Coatings*; Wiley-Interscience: New York, 1982.
[9] Pappav, P. *Radiation Curing, Science and Technology*; Plenum Press: New York, 1992.
[10] Campbell, M.; Sharp, D.N.; Harrision, M.T.; Denning, R.G.; Turberfield, A.J. *Nature* **2000**, *404*, 53–56.
[11] Bunning, T.J.; Natarajan, L.V.; Tondiglia, V.P.; Sutherland, R.L.; Vezie, D.L.; Adams, W.W. *Polymer* **1995**, *36*, 2699–2708.
[12] Hashimoto, T. In *Current Topics in Polymer Science*, Ottenbrite, R.; Utracki, L.A.; Inoue, S. Eds.; Macmillan: New York, 1987
[13] Han. C.C. *Polym. Eng. Sci.* **1986**, *26*, 3–8.
[14] Binder, K. *J. Chem. Phys.* **1983**, *79*, 6387–6409.
[15] Sariban, A.; Binder, K. *J. Chem. Phys* **1987**, *86*, 5859–5873.
[16] Chakrabarti, A.; Torai, R.; Gunton, J.D.; Muthukumar, M. *J. Chem. Phys.* **1990**, *92*, 6899–6909.
[17] Cahn, J.W.; Hilliard, J.E. *J. Chem. Phys.* **1958**, *28*, 258–267.
[18] Cahn, J.W. *J. Chem. Phys.* **1965**, *42*, 93–97.
[19] Cook, H.E. *Acta Metall.* **1970**, *18*, 297–306.
[20] Langer, J.S.; Baron, M.; Miller, D. *Phys. Rev. A* **1975**, *11*, 1417–1429.
[21] Binder, K.; Stauffer, D. *Phys. Rev. Lett.* **1974**, *33*, 1006–1009.
[22] Siggia, E. *Phys. Rev. A* **1979**, *20*, 595–605.
[23] Lifshitz, I.M.; Slyozov, V.V. *Chem. Phys. Solids* **1961**, *19*, 35–50.
[24] Kawasaki, K.; Ohta, T. *Prog. Theor. Phys* **1978**, *59*, 362–374.
[25] Furukawa, H. *Physica A* **1984**, *123*, 497–515.
[26] Dozov, P. *Liquid Crystal Dispersions*; World Scientific Publishing: Singapore, 1995; 1.
[27] Lucchetta, D.E.; Criante, L.; Francescangeli, O.; Simoni, F. *Appl. Phys. Lett.* **2004**, *84*, 4893–4895.
[28] Lucchetta, D.E.; Karapinar, R.; Manni, A.; Simoni, F. *J. Appl. Phys.* **2002**, *91*, 6060–6065.
[29] Nwabunma, D.; Chiu, H-W.; Kyu, T. *Macromolecules* **2000**, *33*, 1416–1424.
[30] Crawford, N.J.; Dadmun, M.D.; Bunning, T.J.; Natarajan, L.V. *Polymer* **2006**, *47*, 6311–6321.
[31] Mucha, S.; Duran, H.; Hu, J.; Kyu, T.; Natarajan, L.V.; Tondiglia, V.P.; Sutherland, R.L.; Bunning, T.J. *Macromolecules* **2007**, *40*, 3190–3197.
[32] White, T.J.; Natarajan, L.V.; Tondiglia, V.P.; Bunning, T.J.; Guymon, C.A. *Macromolecules* **2007**, *40*, 1112–1120.
[33] Duran, H.; Meng, S.; Kim, N.; Hu, J.; Kyu, T.; Natarajan, L.V.; Tondiglia, V.P.; Bunning, T.J. *Polymer* **2008**, *49*, 534–545.
[34] Lucchetti, L.; Simoni, F. *J. Appl. Phys.* **2000**, *88*, 3934–3740.
[35] Kyu, T.; Lee, J.H. *Phys. Rev. Lett.* **1996**, *76*, 3746–3749.
[36] Kyu, T.; Chiu H-W.; Lee, J.H. In *Heterophase Polymer Networks: Synthesis, Characterization and Properties*. Rosenberg, B.A.; Sigalov, G.M., Eds.; Gordon and Breach: Newark, 2001.
[37] Chan, P.K.; Rey, A.D. *Macromolecules* **1996**, *29*, 8934–8941.
[38] Chan, P.K.; Rey, A.D. *Macromolecules* **1997**, *30*, 2135–2143.
[39] Nwabunma, D.; Kyu, T. *Macromolecules* **1999**, *32*, 664–674.
[40] Nwabunma, D.; Chiu, H.; Kyu, T. *J. Chem. Phys.* **2000**, *113*, 6429–6436.
[41] Kyu, T.; Chiu, H. *Polymer* **2001**, *42*, 9173–9185.
[42] Soppera, O.; Croutxe-Barghorn, C.J. *Polym. Sci. Polym. Chem.* **2003**, *41*, 831–840.
[43] Scherzer, T.; Decker, C. *Nucl. Instrum. Methods Phys. Res. B* **1999**, *151*, 306–312.
[44] Decker, C.; Moussa, K. *Macromolecules* **1989**, *22*, 4455–4462.
[45] Lee, T.Y.; Roper, T.M.; Jonsson, E.S.; Kudyakov, I.; Viswanathan, K.; Nason, C.; Guymon, C.A.; Hoyle, C.E. *Polymer* **2003**, *44*, 2859–2865.
[46] Sannier, L.; Siddiqi, H.M.; Maschke, U.; Dumon, M. *J. Appl. Polym. Sci.* **2004**, *92*, 2621–2628.
[47] Kim, J-B.; Lee, M-G.; Choi, J-H. *Polym. Bull.* **1998**, *41*, 37–43.
[48] Fergason, J.L. U.S. Patent 46169035, 1986.
[49] Miyamoto, A.; Morimura, Y.; Kobayashi, S.; Morimura, Y.; Kajiyama, T. *Macromolecules* **1991**, *24*, 3915–3920.
[50] Miyamoto, A.; Kikuchi, H.; Kobayashi, S.; Morimura, Y.; Kajiyama, T. *New Polym. Mater.* **1990**, *2*, 27–40.
[51] Kalkar, A.K.; Kunte, V.V.; Deshpande, A.A. *J. Appl. Polym. Sci.* **1999**, *74*, 3485–3491.
[52] Reamey, R.H.; Montiya, W. *Proc. SPIE.* **1992**, *1665*, 2–7.
[53] Doane, J.W.; Bahadur, B. In *Liquid Crystals: Applications and Uses*; World Scientific: Singapore, 1990, 1, 361.
[54] Yamagishi, F.G.; Miller, L.J. *Van Ast CI. Proc. SPIE.* **1989**, *1080*, 24–31.
[55] Pogue, R.T.; Natarajan, L.V.; Siwecki, S.A.; Tondiglia, V.P.; Sutherland, R.L;. Bunning, T.J. *Polymer* **2000**, *41*, 733–741.
[56] Natarajan, L.V.; Shepherd, C.K.; Brandelik, D.M.; Sutherland, R.L.; Chandra, S.; Tondiglia, V.P. *Chem. Mater.* **2003**, *15*, 2477–2484.
[57] Choa, Y.H.; Kawadea, R.; Kubotab, T.; Kawakami, Y. *Sci. Technol. Adv. Mater.* **2005**, *6*, 435–442.
[58] Boots, H.M.J.; Kloosterboer, J.G.; Serbutoviez, C.; Touwslager, F.J. *Macromolecules* **1996**, *29*, 7683–7689.
[59] Challa, S.R.; Wang, S.-Q.; Koenig, J.L. *Appl. Spectrosc.* **1995**, *49*, 267–272.
[60] McFarland, C.A.; Koenig, J.L.; West, J.L. *Appl. Spectrosc.* **1993**, *47*, 321–329.
[61] Treado, P.J.; Levin, I.W.; Lewis, E.N. *Appl. Spectrosc.* **1992**, *46*, 553–559.
[62] Bhargava, R.; Wang, S.-Q.; Koenig, J.L. *Appl. Spectrosc.* **1998**, *52*, 323–328.
[63] Kim, J.Y.; Palffy-Muhoray, P. *Mol. Cryst. Liq. Cryst.* **1991**, *203*, 93–100.